RAL-TR-2001-009

THE PIN PIXEL DETECTOR - X-RAY IMAGING

J.E. Bateman, J.F. Connolly, G.E. Derbyshire, D.M. Duxbury, A.S. Marsh,
J.E. Simmons and R. Stephenson

Rutherford Appleton Laboratory, Chilton, Didcot, Oxon, OX11 0QX, U.K.

12 January 2001

Abstract

The development and testing of a soft x-ray gas pixel detector, which uses connector pins for the anodes is reported. Based on a commercial 100 pin connector block, a prototype detector of aperture 25.4mm x 25.4mm can be economically fabricated. The individual pin anodes all show the expected characteristics of small gas detectors capable of counting rates reaching 1MHz per pin. A 2-dimensional resistive divide readout system has been developed to permit the imaging properties of the detector to be explored in advance of true pixel readout electronics.

1. Introduction

Imaging gas counters based on Multi-Wire Proportional Counter (MWPC) technology have a long history of successful application to x-ray diffraction [1-7]. Their properties of low noise, high detective quantum efficiency and the large dynamic range of counting detectors have continued to make gas detectors attractive for application on Synchrotron Radiation (SR) beam lines. In general the spatial resolution (standard deviation, σ) achieved lies in the range of 1/1000 to 1/2000 of the working aperture of the detector.

As the brilliance of SR beam lines has increased, the difficulty of reading out the MWPC detectors fast enough has become a challenging problem. Wire counters are, by their very nature projective readout devices which demand that every event passes through the common, global readout system. When the global data rate of the detector exceeds 1MHz, the electronic systems required become extremely complex and expensive [7]. Given the present state of development of microelectronics the possibility of economically instrumenting a gas pixel detector appears to be viable. In this case each small pixel detector will have its own amplification, discrimination and storage attached to it and so be capable of taking data at rates approaching 1MHz, leading to a potential global rate capability in the range of hundreds of GHz.

In a gas counter, the useful size of a pixel is determined by the detection processes in the gas. At x-ray energies of <10keV one can almost neglect the spatial broadening due to the range of the primary photoelectron and the spatial extent of the electron cloud at the detector plane is determined by the diffusion which takes place in the x-ray conversion space or drift gap. In a practical detector the drift gap generally lies between 10mm and 30mm and the gas pressure is from 1bar upwards. In the best argon-based mixtures at 1bar with the optimum drift electric field value, a 10mm drift results in a gaussian distribution of 0.5mm FWHM and a 30mm drift gives a footprint on the detector plane with a FWHM of 0.8mm [8]. With xenon (instead of argon), or with inferior quench gases or non-optimal drift fields these figures degrade, while increasing the gas pressure can improve them (provided the drift field is optimised).

If the pixel dimension is less than the footprint of the charge cloud hitting the detector plane then the charge of one event will be distributed between many pixels each of which will receive a small fraction of the total charge. This results in a very poor pulse height distribution in any one pixel and a large triggering multiplicity. For example if one considers the recently proposed gas pixel detectors made by lithographic techniques such as the microdot detector [9] one finds that with a pixel diameter of 0.2mm one x-ray event will trigger >4 channels with a 10mm drift and >16 channels with a 30mm drift. The Multi Pin Array Detector [10] has a more useful dimension with a 0.6mm hexagonal cell diameter. However, even in this case there will be essentially no events in which the charge is not shared between two or more channels with a 10mm drift.

Experience with the Gas Microstrip Detector (GMSD) (a linear detector) has shown that with a strip width of 10σ (i.e. 2mm) and a drift distance of 10mm, only 35% of the events lie in the full energy peak for 5.9keV x-rays. This fraction is considerably lower in the case of a pixel detector where four edges contribute instead of only two, so it is not possible to have a practical pixel size which will give x-ray energy

resolution without summing over many pixels. This demands some form of global or semi-global readout, which returns the readout to the rate limits typical of the MWPC. A compromise pixel size is thus required which will trigger at most a small number (two or three) pixels per event and yet be small enough to keep the detector aperture within reasonable bounds. Such a compromise pixel size is ≈1mm. At this pixel dimension it is possible to use electronic circuit connector pins as anodes as introduced by one of the authors [11]. Today it is possible to obtain a one inch square array connector with precision pins spaced on a pitch of 0.05inch (1.27mm) [12]. With a detector aperture of 500mm this gives a resolution of 1/1364 of the aperture (σ = 0.37mm). This report describes the development and performance of a prototype of a gas pixel detector based on such a connector array. As a first step a single connector array (25.4mm x 25.4mm) of pitch 0.1inch (2.54mm) was used.

2. The Pin Detector

2.1 History

The use of point anodes in gas counters has a long history which is well described in reference [13]. The general plan was to use short wires or needle tips with radii comparable with the radius typically used in a conventional wire counter, i.e. a few tens of microns. As shown elsewhere [11] the gain process of such an anode passes very quickly into a Self Quenching Streamer (SQS) mode resulting in very large, fast pulses which exhibit severe dead time limitation. Using an anode with a radius of the order of 0.5mm has been shown [11] to result in stable, proportional amplification with adequate gas gain for practical readout purposes (>10 000). The connector pins used in the prototype pixel detector meet this requirement having a diameter of 0.64mm with a spherical end.

Comby and Mangeot [14] introduced a cathode focussing grid in front of an array of fine needles to make a pixel detector operating in SQS mode and capable of detecting UV-generated single electrons. Adapting this structure to linear operation with x-rays, Bateman and Connolly developed a prototype pixel detector by mounting loose connector pins in a 10 x 10 array on a 2.54mm pitch [15]. A serious problem with this approach was the variability of the pin dimensions which led to a rather large fluctuation in the pixel to pixel gain. As will be seen, the availability of the 100-pin connector array solves this problem.

2.2 Design

Figure 1 shows a schematic cross-section of the present prototype pin pixel detector. The 100-pin connector array is mounted in a Macor plate which locates it and spaces it so that the anode pins are accurately positioned within the matching holes in the brass cathode (base) plate. A drift electrode consisting of aluminised mylar stretched on a GRP frame is spaced 10mm in front of the cathode plate. Electrical connection between the back of the 100 anode pins and the readout assembly is made via a second pin array. The gold-plated brass pins of the connector array are moulded into a polyester base with great precision. A survey of the pin tips showed them to be accurately on a 2.54mm planar grid within an error of 10 microns in all three dimensions. The various layers of the anode/cathode structure are keyed together with

dowels to ensure positional (and therefore gain) uniformity. Figure 2 shows the magnified appearance of a portion of the cathode as viewed from the drift space. The holes in the cathode plane are slightly counter-sunk to avoid sharp edges around the pins.

The Macor mounting electrically isolates the pin array which is maintained at earth potential while the cathode is typically held at ≈ -1400V (V_c) and the drift cathode (V_d) is held at a few hundred volts more negative than V_c. The structure of figure 1 is held in a gas-tight enclosure with a thin aluminised mylar window above the drift electrode to permit entry of the x-rays. Gas ports and electrical sockets are provided for interface to the readout system. For the present tests a flowed gas filling of argon + 25% isobutane was used.

2.3 Operating Characteristics

Collimating a beam of 5.9keV x-rays (from a ^{55}Fe source) onto a single pin with operating conditions V_c = -1350V and V_d = -1450V produces the pulses shown in figure 3 when the pin is connected to a fast current-sensitive preamplifier. When the pin is connected to a charge preamplifier / main amplifier / pulse height analyser chain, the typical gas counter pulse height distribution of figure 4 is observed with a FWHM energy resolution of 19.1%.

The x-rays can be used to calibrate the gas gain in the usual way. Figure 5 shows the typical gas counter gain curve (gain versus V_c) with gains of >10 000 available. Also shown is the FWHM energy resolution of 5.9keV x-rays as a function of V_c.

It is important for the uniformity of response of the detector that the gain variation from pin to pin is not excessive. Figure 6 shows a histogram of the peak channel of the x-ray line as obtained from all 100 pins. The distribution is approximately normal with a standard deviation (σ) of 6.8%. This level of dispersion is very acceptable and the normal distribution tends to indicate that no single error in the pin alignment set-up is dominant. When the whole counter is irradiated the resulting FWHM energy resolution is degraded by the gain variation from ≈19% to ≈25%.

Because of the large area of cathode surface relative to the pin-holes, the drift field in the pin detector is quite critical in determining its energy resolution and effective gain. At higher drift fields (≈400V/cm) charge from events is drawn down onto cathode between the holes and is lost to the pin amplification process. This leads to a degradation of the pulse height spectrum seen in figure 4 with a distribution of small pulses tailing to low values. However, at low drift fields (≈100V/cm), unless the gas is extremely clean, electron attachment reduces the size of the cloud reaching the pin and the energy FWHM deteriorates. Figure 7 shows these effects via a plot of the (apparent) gain and energy FWHM as a function of the drift potential (V_d) at fixed V_c. The region of rapidly rising gain and falling FWHM corresponds to the region in which electron attachment is strongly felt. At V_d = -1550V the minimum in the FWHM is reached. Above this value of V_d the apparent gain rises more slowly, according to the behaviour observed for gas microstrip detectors (GMSD) [16] with a ΔV_d change in V_d equivalent to a $0.03\Delta V_d$ in V_c (i.e. the gain is relatively insensitive to V_d). The use of a less electronegative gas mixture (e.g. argon + 10% methane) will significantly reduce the electron attachment effects seen in figure 7.

2.4 Rate Capability

The rate performance of the whole detector is essentially governed by the rate performance of each individual pin. Figure 8 shows the typical behaviour of the gain of an individual pin as a function of the counting rate on it. A 20% loss of gain is observed relative to the value at low rate (M = 15 000) at a detected rate of 100kHz. The gain loss is always proportional to the magnitude of the charge pulse delivered by the pin, in this case $Q_0 = 3x10^6$ electrons. This is a very large signal and at least a factor of ten greater than would be used in a typical pixel readout amplifier. With $Q_0 = 1x10^5$ electrons the gain drop will be 2% at 100kHz and 20% at 1MHz. This performance matches well to the speed of economic counting pixel electronics and will comfortably meet the requirements for a high rate SR detector (≈100GHz global capability).

3. The Readout

The ideal readout method for the pin pixel detector is, naturally, one in which each anode is individually instrumented so that maximal benefit can be had from the rate capability of each anode. However, for test purposes (and potentially as a medium rate general purpose readout) a global analogue readout of the 25.4mm x 25.4mm tile was implemented. Since charge division electronics were available from a preceding programme [17] readout was arranged by means of a resistive pad. A readout board is coupled to the anode pin array (figure 1) in which each anode is coupled to its neighbour by a 2kohm surface mount resistor. At each edge of the array a bus bar collects the charge leaving each row and column via a weighted resistor network. A charge pre-amplifier is connected to each of the four bus bars and after amplification and shaping of the pulses, the pseudo x and y co-ordinates:

$$X = \frac{(L-R)}{(L+R)} \quad \text{and} \quad Y = \frac{(T-B)}{(T+B)} \qquad (1)$$

are calculated in an analogue computer and fed to a digital data capture system. L and R represent the pulse heights available from the left and right bus bars and T and B those from the top and bottom bus bars. Tests have shown that this readout can function with excellent precision up to data rates of 400kHz in a linear readout [17]. The time constant of the anode pad readout in use with the pin array (≈1.5μs) limits this maximum rate to ≈100kHz and sets a limit of this order to the readout rate from a tile of 100 pins.

Figure 9 shows the digital image obtained from this readout when the detector is flooded with x-rays. The 100 pins are all clearly resolved with a small degree of distortion introduced by the simplified charge division algorithm. The pin matrix provides an intrinsic calibration of this distortion and facilitates off-line image rectification. The data was captured in a standard PC using the National Instruments LabView software and hardware. Figure 10 shows a histogram of the Y values for a column of pins in figure 9.

As with all analogue readout systems, the dynamic range of the pulse must be controlled to ensure a uniform response. In the present system this control is applied by pulse height selection of the sum of the four signals (L+R+T+B). Depending on the nature of the spectrum this process can result in a loss of events amounting to a few percent to a few tens of percent.

4. Imaging Performance

The imaging performance of the prototype detector is partially determined by the physics of the detection process and partially by the properties of the analogue readout system. Since the analogue readout automatically interpolates the signals generated on adjacent pins, events near the pixel boundary which spread by diffusion into the neighbouring pixel will be assigned an intermediate X value (or Y, as may be the case). As figure 10 shows, at low drift field (≈100V/cm) many more events share their charge compared with those detected with high field (≈400V/cm).

In order to investigate the spatial response function of the detector in detail a collimated slit x-ray beam was set up which had a FWHM of 1.1 mm in the narrow dimension in the middle of the 10mm drift space of the detector and a length of ≈10mm. The detector was placed on a precision scanning table and moved through the beam transverse to the slit beam. The digital images of the slit taken at scan table positions spaced at 0.5mm were converted into one-dimensional histograms across the slit beam. Figure 11 shows a selection of such histograms (in the pseudo co-ordinate Y) recorded with low drift field and showing varying degrees of interpolation.

Figure 12 shows the centroids of the Y histograms plotted against the scan table position. A perfect pixel definition would result in a simple staircase function. Figure 12 shows such a function convolved with the spread of the diffusion function and the beam width. Approximate calculation of the diffusion indicates that the FWHM of the diffusion footprint is ≈0.5mm. Taking this as the distance from the pixel boundary over which sharing will occur predicts flat steps of 1.5mm width with a transition region of 1mm between each step. This is essentially what is observed in figure 12. That no events are lost in the transition region is demonstrated by the plot in figure 13 in which the total counts in the distribution are counted and plotted for each scan position. The standard deviation of 3.3% measured across the three pins is consistent with the variation to be expected from the distribution of pin gains shown in figure 6 and gives an estimate of the differential non-linearity of the system.

An estimate of the diffusion footprint can be obtained by averaging all the 13 histograms (taken at the various scan positions) after normalising them to their individual centroid Y values. The result is shown in figure 14. The averaging of the gaussian diffusion response over the drift depth results in a curve which is fitted with a sum of two gaussians with FWHMs of 0.43mm and 1.25mm. This is in approximate accord with expectation from the known diffusion properties and the beam width.

The measurements displayed in figures 11 to 14 were all made near the centre of the detector where the spatial response is most linear. The calibration of the Y measure in terms of the space defined by the pin spacing (y) is taken from the pin spacing near the centre. Thus the slope of the calibrated Y measure (y') versus the scan table

position should be –1 in figure 12. In fact it is –0.855, showing that over the span of 5mm about centre field some non-linearity is evident.

The effect of the diffusive interpolation on the flood response is observed in figure 9 as weak lines of events connecting the pin peaks. No events are missing in the corner positions, the readout simply interprets them as lying on one of the axial lines. Thus the point response for a uniformly illuminated pixel is a central peak with a weak star-like pattern along the readout axes. After the image is rectified the events in a pixel can be simply evaluated as the sum of the peak plus all the "bar" events within ±0.5 pixel widths along each axis.

Figure 15 shows the response of the detector to the x-ray image formed by a circular ring mask of inner diameter 17mm and outer diameter 21mm illuminated by the 5.9keV x-ray source placed 300mm distant. Two of the quadrants of the circle lie within the 1.5mm flat-response pixel width and two lie in the 1mm interpolation zone. The curvature of the circle is thus only indicated in the arcs which experience interpolation.

5. Discussion

The properties of the basic pin pixel detector, as exhibited in figures 3 to 8 above, show that each pin is capable of functioning as a very high rate x-ray detector with sufficient gain to drive either a pixellated readout or some form of compromise analogue system such as that used to test the prototype. The charge division readout system has confirmed the interpolative effect expected from the diffusion of the primary electron clouds. With a 2.5mm pixel ≈40% of events in a flood field bring up a single pixel while the remainder register in two adjacent pixels. The implication of the readout studies is that very few events register in more than two pixels.

Construction and operation of the prototype detector was simple and reliable. The operating characteristics did not change significantly when new connector arrays were substituted for the original one. This indicates that detectors made from a tiling of many arrays is feasible. The main problem encountered was that occasionally a connector array was found to have a burr left from machining on the tip of a pin. This would declare itself after a running period by becoming noisy due to the build-up of hydrocarbon deposit from the quencher on the burr. Inspection of arrays before insertion into a large area counter will probably be necessary.

A design programme has been initiated for integrated electronics for true pixel readout of this and other similar detectors. It is hoped to include all amplification, discrimination and data storage for 64 channels on a single silicon chip, thus opening the way to the GHz global rates promised by the individual pin performance. While sacrificing two orders of magnitude in global readout rate potential, the use of a hybrid analogue readout, such as that used with the prototype, may offer a half-way house in the development of very high rate x-ray diffraction detectors.

Design and construction of a second prototype using the 0.05inch pitch pin array is in hand. This poses several new challenges in the mechanical construction and the readout design, none of which are seen to be insuperable.

References

1. C. Cork, D. Fehr, R Hamlin, W. Vernon, N. Huu Xuong and C. Perez-Mendez, J. App. Cryst. (1973) **7**, 319

2. M.E. Andianova, D.M. Kheiker, A.N. Popov, V.I. Simonov, Yu.S. Anisimov, S.P. Chernenko, A.B. Ivanov, S.A. Movchan, V.D. Peshekhonov and Yu.V. Zanevsky, J. App. Cryst. (1982) **15**, 626

3. R. Kahn, R. Fourme, R. Bosshard and V. Saintagne, Nucl. Instr. and Method **A246** (1986) 596

4. R.P. Phizackerley, C.W. Cork and E.A.Merritt, Nucl. Instr. and Method **A246** (1986) 579

5. J.E. Bateman, J.F. Connolly, R. Stephenson, C.J. Bryant, A.D. Lincoln, P.A. Tucker and S. Swanton, Nucl. Instr. and Method **A259** (1987) 506

6. G.C. Smith, B. Yu, J. Fischer, V. Radeka and J.A. Harder, Nucl. Instr. and Method **A323** (1992) 78

7. R.A. Lewis, W.I. Helsby, A.O. Jones, C.J. Hall, B. Parker, J. Sheldon, P. Clifford, M. Hillen, I. Sumner, N.S. Fore, R.W.M. Jones and K.M. Roberts, Nucl. Instr. and Method **A392** (1997) 32

8. A. Peisert and F. Sauli, Drift and diffusion of electrons in gases: a compilation, CERN 84-08 (1984)

9. S.F. Biagi, J. Bordas, D. Duxbury, E. Gabathuler and T. Jones, Nucl. Instr. and Method **A336** (1995) 76

10. P. Rehak, G.C. Smith, J.B. Warren and B. Yu, Micro Pin Array Detector (MIPA) : First test results, Proceedings of the International Workshop on Micro-Pattern gas Detectors, Orsay, France, June 28-30, 1999, p11

11. J.E. Bateman, Nucl. Instr. and Method **A238** (1985) 524

12. ADVANCED Interconnections Catalogue

13. G. Comby et. al., CEN-Saclay Report DPhE/STIPE 79/01/02/36

14. G. Comby and P. Mangeot, IEEE Trans. Nucl. Sci. NS-27 (1980) 106

15. J.E. Bateman and J.F. Connolly, A gas pixel detector for x-ray imaging, Proceedings of the European Workshop on X-ray Detectors for Synchrotron Radiation Sources, Aussois, France, September 30 – October 4, 1991, p92

16. J E Bateman, J F Connolly, G E Derbyshire, D M Duxbury, J Lipp, J A Mir, R Stephenson, J E Simmons and E J Spill, Studies of the gain properties of gas microstrip detectors relevant to their application as x-ray and electron detectors, RAL-TR-1999-057 (http://www-dienst.rl.ac.uk/library/1999/tr/raltr-1999057.pdf) (A shortened version is published in the Proceedings of the International Workshop on Micro-Pattern Detectors, Orsay, France, 28-30 June 1999)

17. J E Bateman, J F Connolly, A B Lodge, R Stephenson, R Mutikainen, I Suni and J Morse, A gas microstrip detector for x-ray imaging with readout of the anode by resistive divide, Presented at the 5th International Conference on Position Sensitive Detectors, University College London, 13-17 September 1999

Figure Captions

1. A schematic cross-section of the prototype pin pixel detector showing the essential elements. The gas containment vessel is not shown.

2. A photograph of a small portion of the pin array assembly as viewed from the drift space of the detector.

3. The current pulses delivered by a single pin of the pin pixel detector when irradiated by ^{55}Fe x-rays. The gas gain is ≈10 000 in an argon + 20% methane mixture.

4. The charge pulse height spectrum produced from a single pin of the pin pixel detector when irradiated by ^{55}Fe x-rays under the conditions indicated. Drift space = 10mm.

5. The gain and x-ray energy resolution as a function of the cathode potential (V_c) with the drift potential (V_d) held 100V negative of V_c.

6. A histogram of the peak channel of the x-ray pulse height distributions (i.e. gains) for all 100 pins of a single array.

7. A plot of the apparent gas gain of a single pin (i.e. including attachment losses) and the x-ray energy resolution as a function of V_d with V_c fixed.

8. The relative gain of a single pin as a function of rate under the conditions shown. The fit curve has no physical significance but is useful for interpolation.

9. The flood response of the pin pixel detector to ^{55}Fe x-rays as captured by the resistive divide readout and the digital data capture system. With a 30mm drift gap, V_c = -1350V and V_d = -2700 (high drift field) and pulse height selection operating.

10. Y histograms of the 5th column of pins in figure 9, showing the change in the amount of interpolation between the cases of low drift field (≈100V/cm) and high drift field (≈400V/cm).

11. Typical Y histograms obtained as the pin pixel detector is scanned through the slit x-ray beam across the space between three pins (5mm). YSCAN is the position of the scanning table.

12. A plot of the measured position of the centroids of the histograms in figure 11 (y') as a function of the scan table position (y).

13. The total counts in each Y histogram at each scan table position is plotted against position.

14. After transforming the individual Y histograms (figure 11) to the variable $y' - y'_m$ where y'_m is the centroid of each distribution, they are all averaged together to produce this plot.

15. The response of the pin pixel detector to a ring beam of ^{55}Fe x-rays.

FIGURE 1

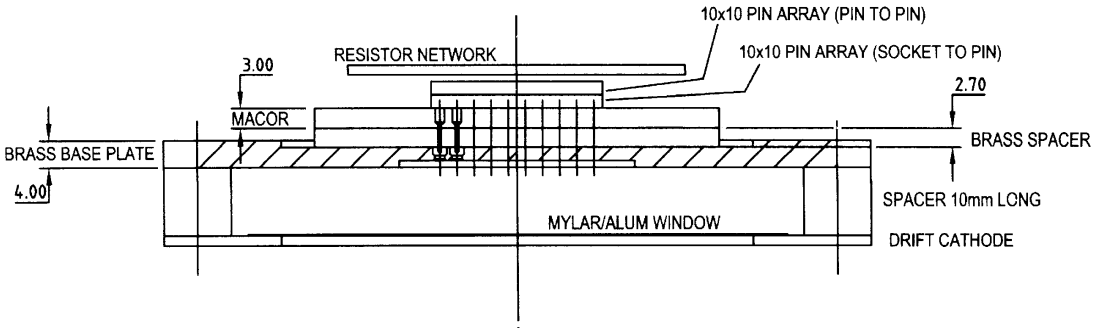

FIGURE 2

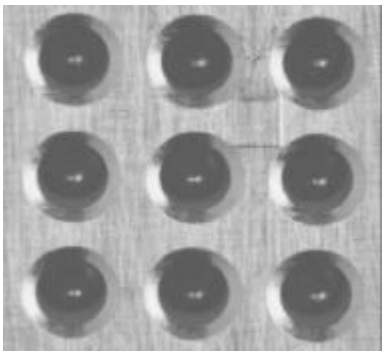

FIGURE 3

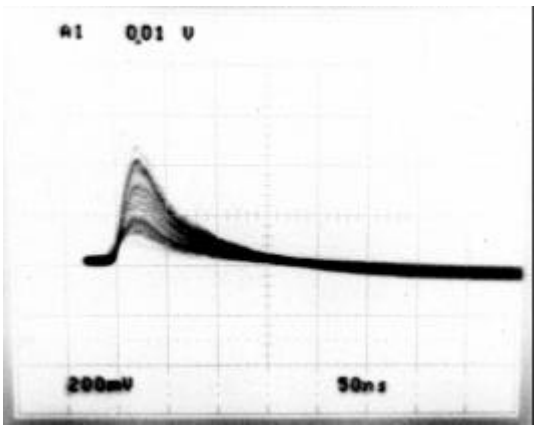

FIGURE 4

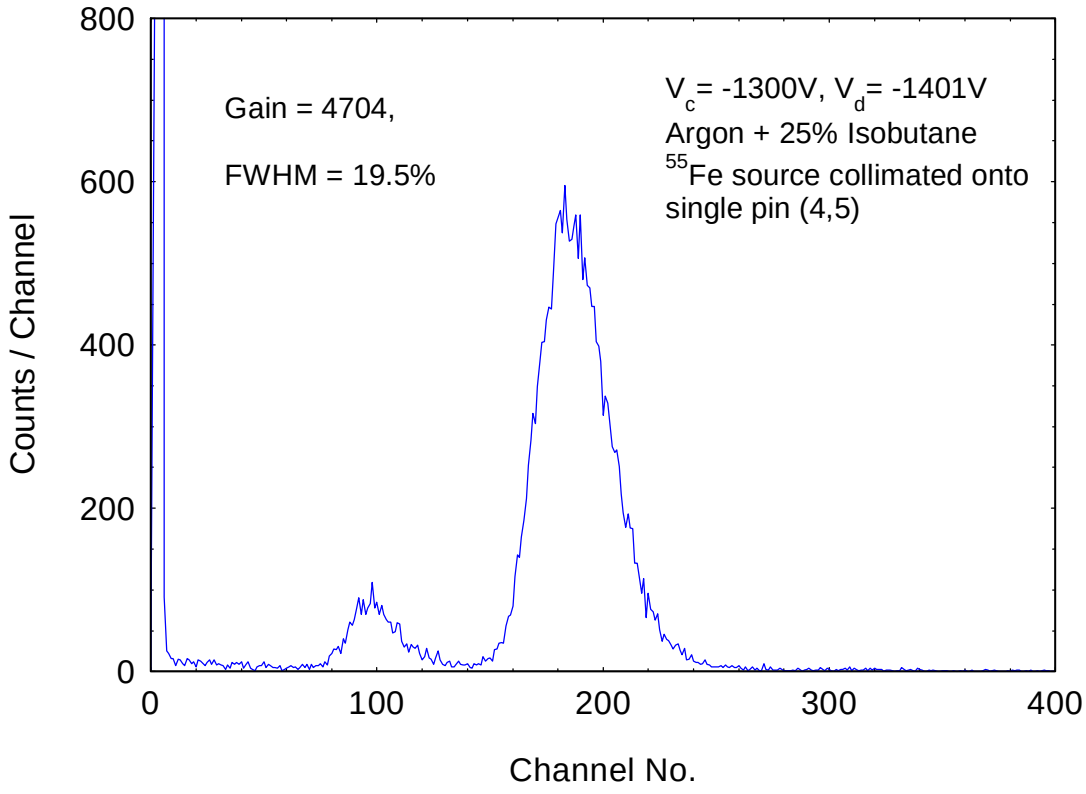

FIGURE 5

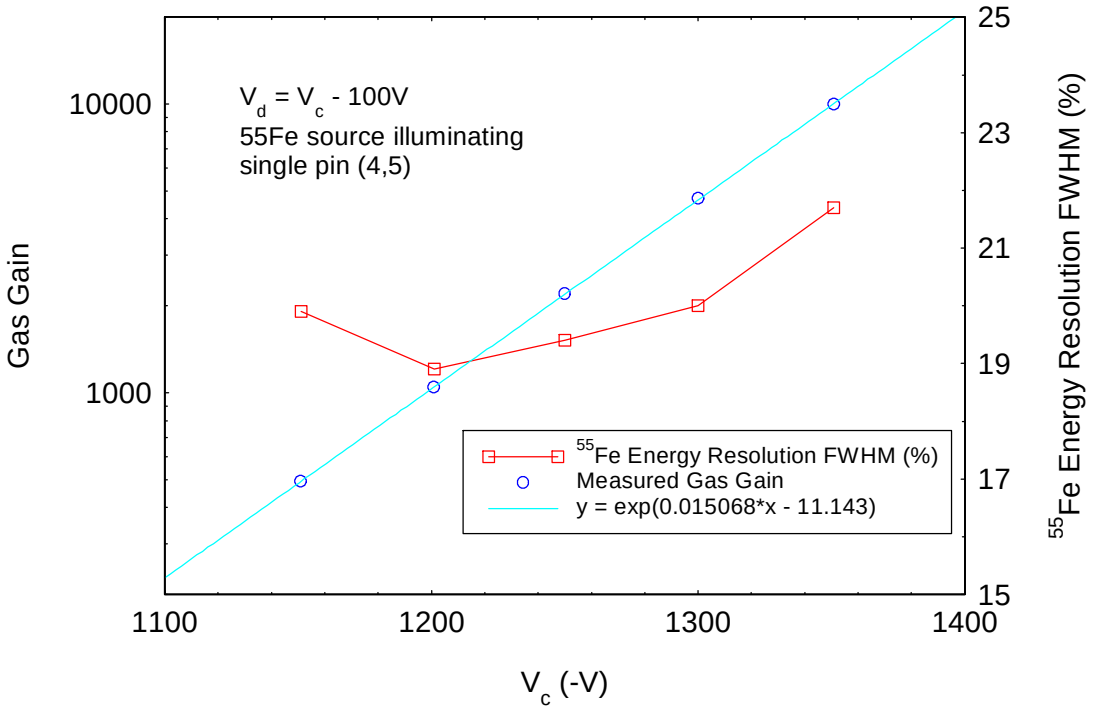

FIGURE 6

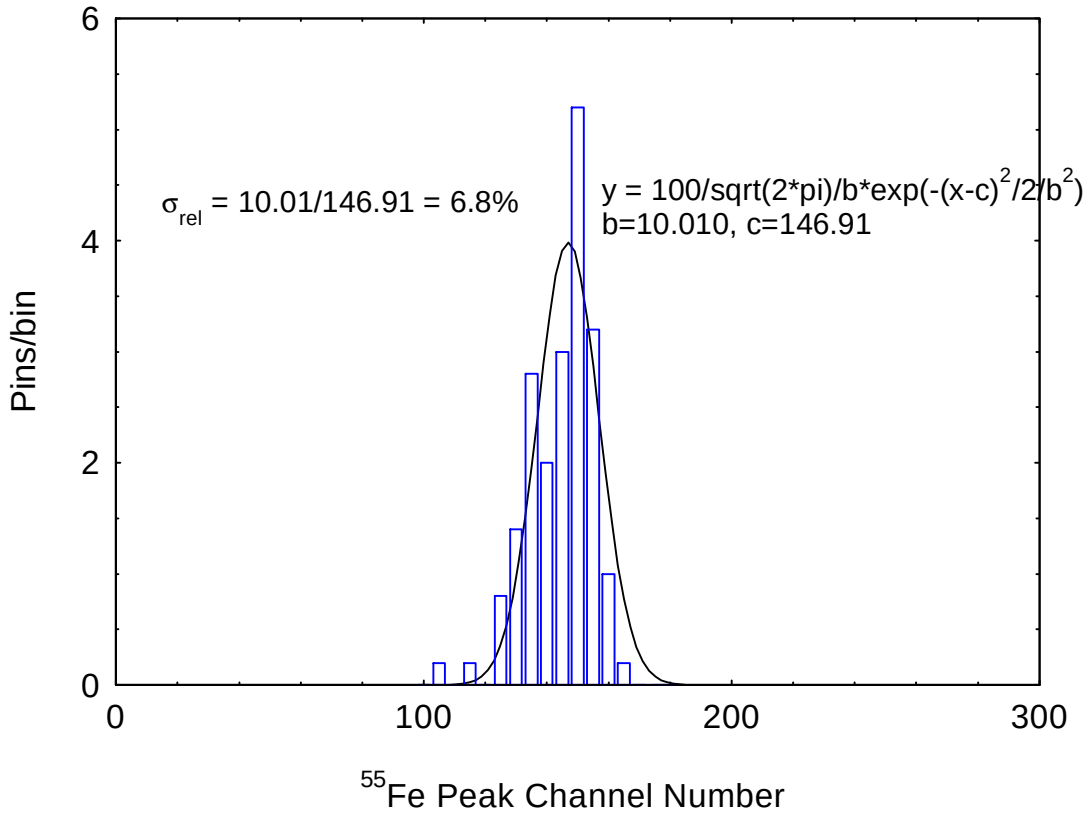

FIGURE 7

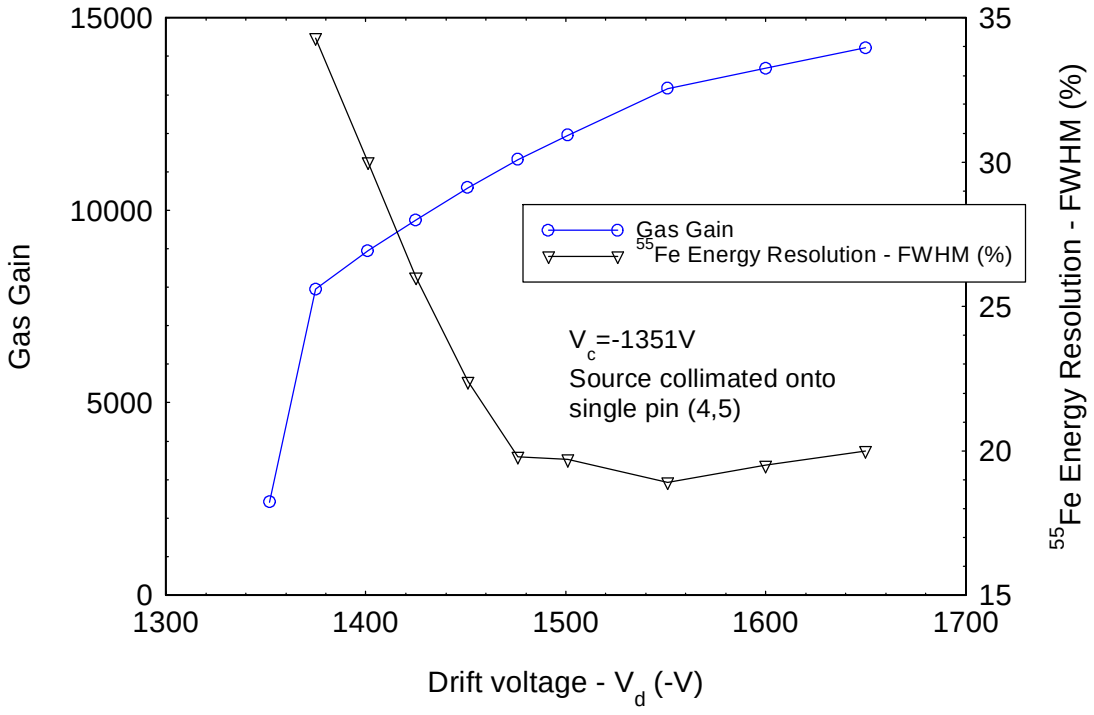

FIGURE 8

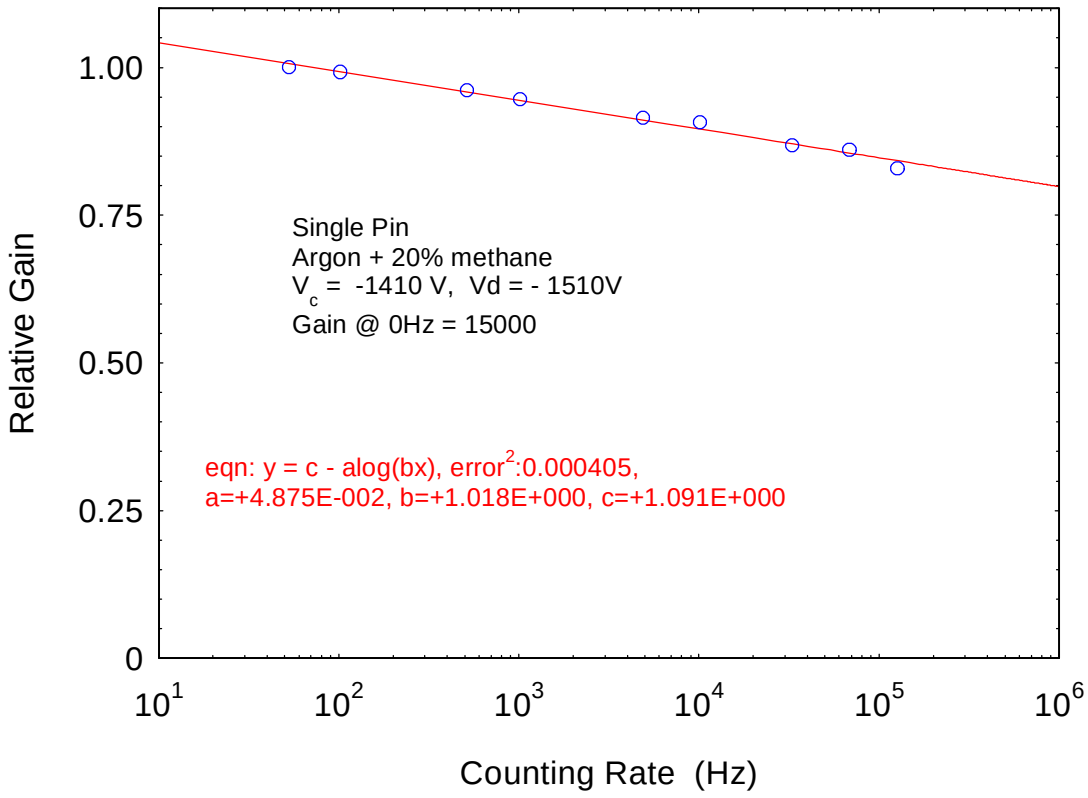

FIGURE 9

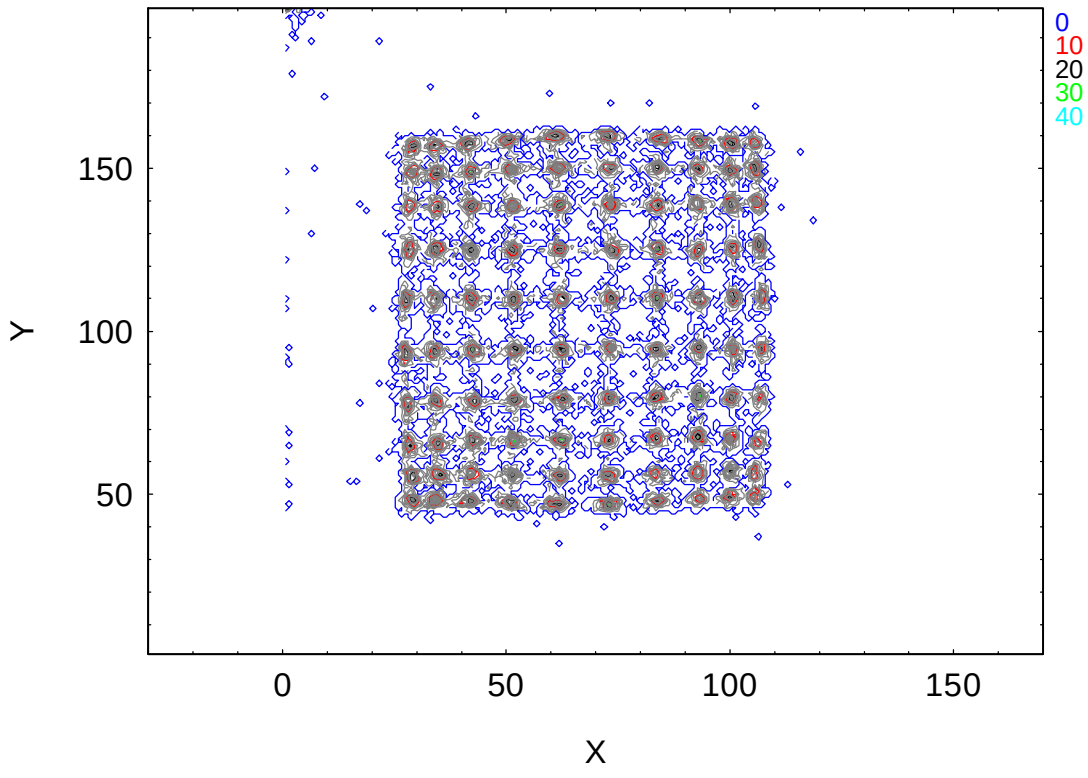

FIGURE 10

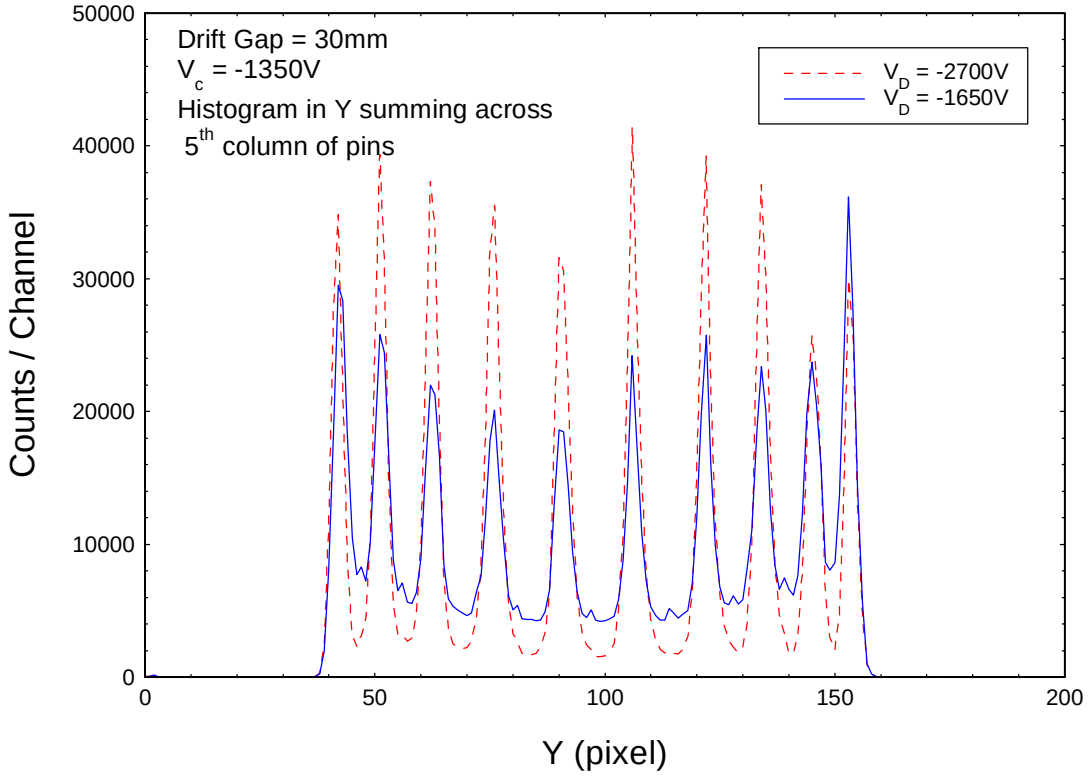

FIGURE 11

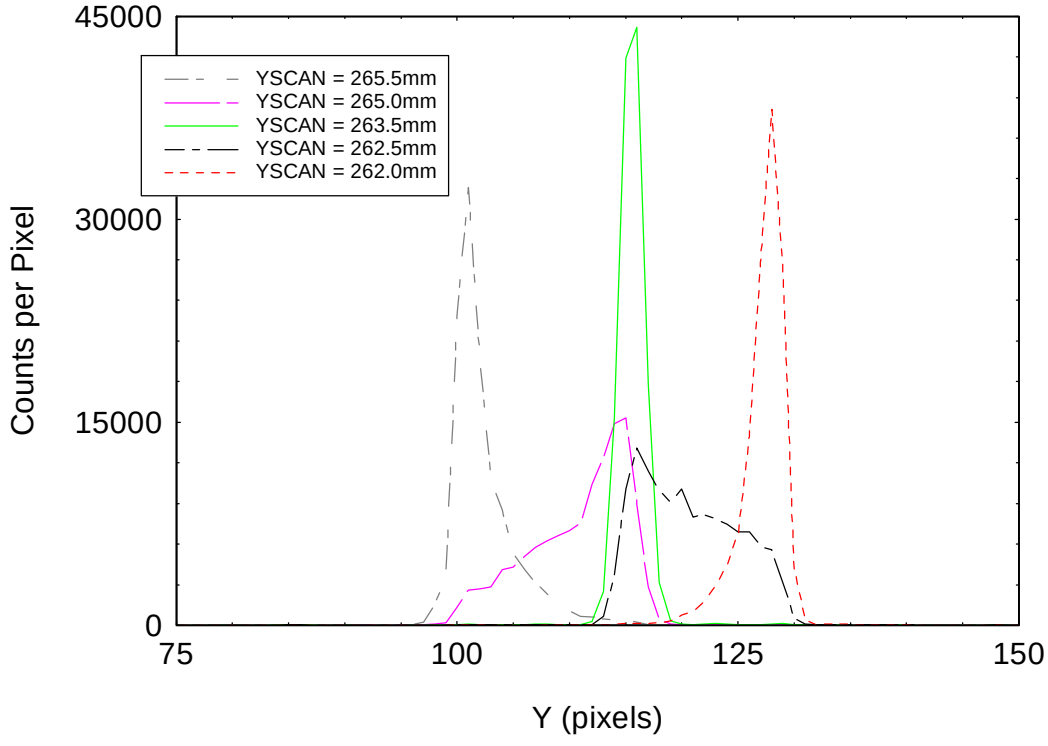

FIGURE 12

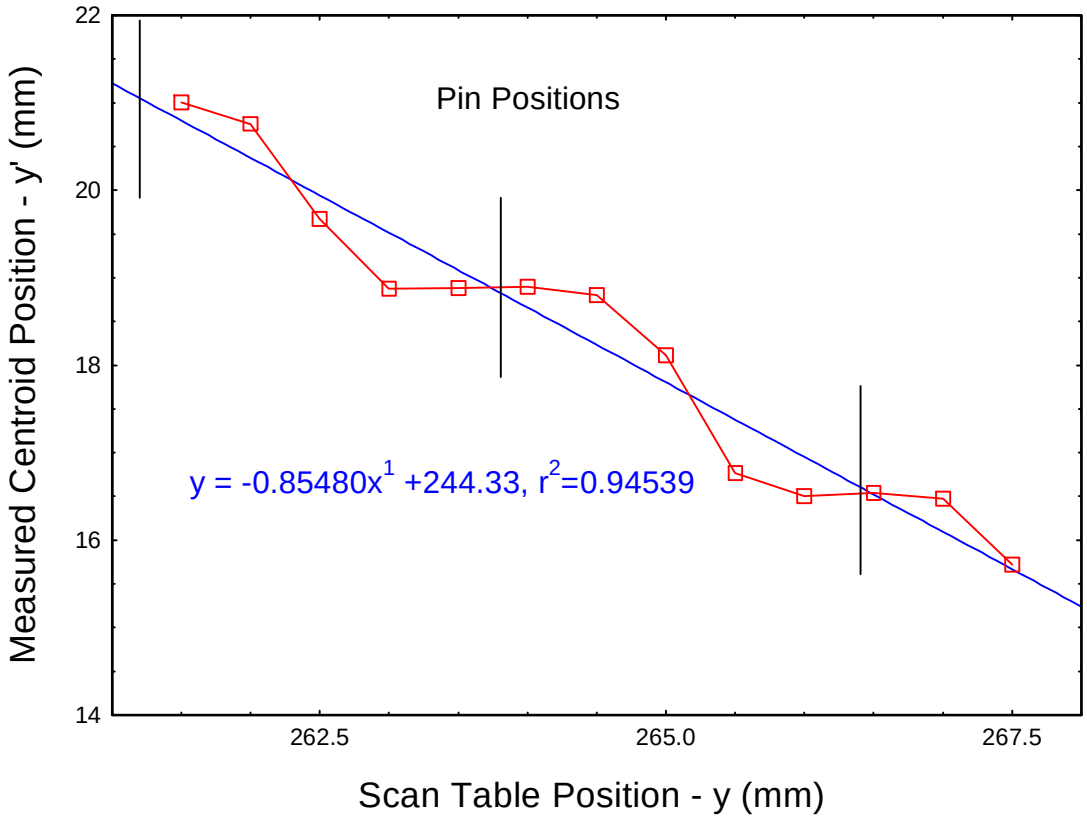

FIGURE 13

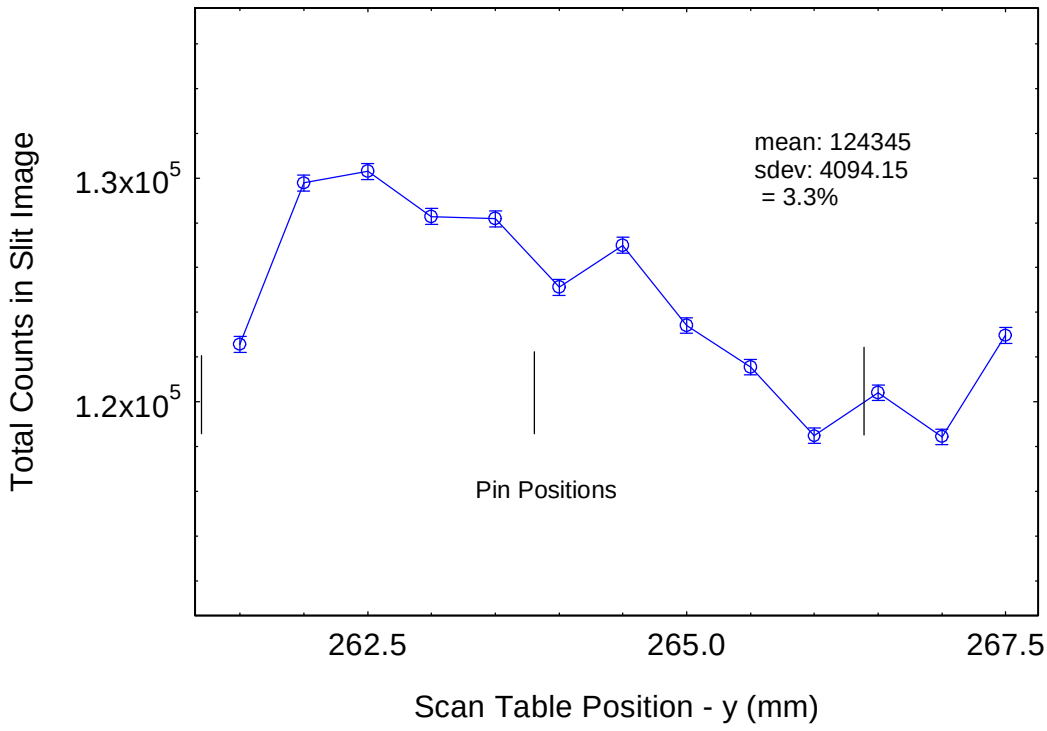

FIGURE 14

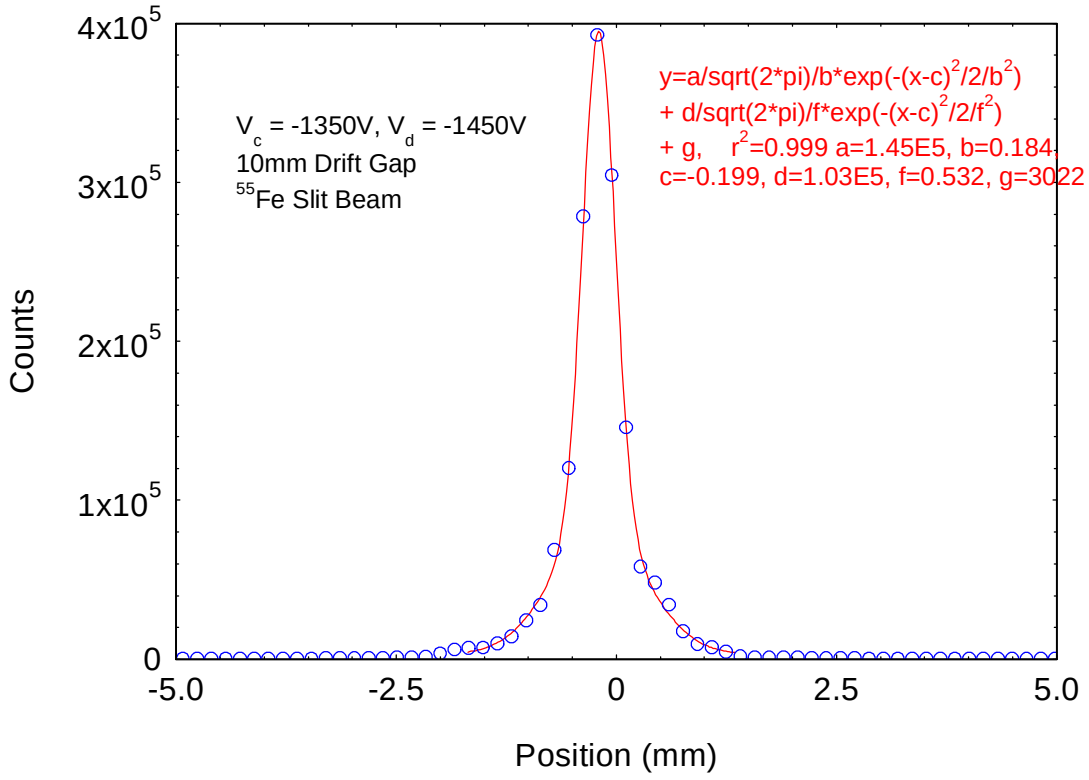

FIGURE 15